nature cell biology

BMI1 represses *Ink4a/Arf* and *Hox* genes to regulate stem cells in the rodent incisor

Brian Biehs[1,2,6,7], Jimmy Kuang-Hsien Hu[1,6], Nicolas B. Strauli[1], Eugenio Sangiorgi[3,7], Heekyung Jung[4], Ralf-Peter Heber[1], Sunita Ho[5], Alice F. Goodwin[1], Jeremy S. Dasen[4], Mario R. Capecchi[3] and Ophir D. Klein[1,2,8]

The polycomb group gene *Bmi1* is required for maintenance of adult stem cells in many organs[1,2]. Inactivation of *Bmi1* leads to impaired stem cell self-renewal due to deregulated gene expression. One critical target of BMI1 is *Ink4a/Arf*, which encodes the cell-cycle inhibitors $p16^{Ink4a}$ and $p19^{Arf}$ (ref. 3). However, deletion of *Ink4a/Arf* only partially rescues *Bmi1*-null phenotypes[4], indicating that other important targets of BMI1 exist. Here, using the continuously growing mouse incisor as a model system, we report that *Bmi1* is expressed by incisor stem cells and that deletion of *Bmi1* resulted in fewer stem cells, perturbed gene expression and defective enamel production. Transcriptional profiling revealed that *Hox* expression is normally repressed by BMI1 in the adult, and functional assays demonstrated that BMI1-mediated repression of *Hox* genes preserves the undifferentiated state of stem cells. As *Hox* gene upregulation has also been reported in other systems when *Bmi1* is inactivated[1,2,5–7], our findings point to a general mechanism whereby BMI1-mediated repression of *Hox* genes is required for the maintenance of adult stem cells and for prevention of inappropriate differentiation.

A central goal in stem cell biology is to understand the mechanisms of tissue regeneration and renewal used by diverse organs. In the case of the rodent incisor, continuous growth relies on stem cells that share several characteristics with other regenerating adult systems[8–11]. These include residence in a discrete niche, slow division kinetics with respect to surrounding cells, and the ability to give rise to differentiated lineages throughout the life of the animal. Label-retaining experiments in mice using either BrdU incorporation or genetic labelling with a tetracycline inducible histone 2B–GFP (H2BGFP) reporter demonstrated that a population of slowly dividing epithelial stem cells was present in a structure called the labial cervical loop (LaCL) at the proximal end of the incisor[8,12]. Lineage tracing experiments showed that these cells gave rise to the highly proliferative transit-amplifying (T-A) cells that then differentiated into enamel-secreting ameloblasts[11–13]. Genetic analyses have shown that development of the incisor stem cells is controlled by TGF-β/BMP and FGF signalling[9,10] and that adult stem cells require active SHH signalling to produce differentiated progeny[12]. However, it remains relatively unknown how homeostasis is regulated in the adult LaCL. As *Bmi1* plays a key role in adult stem cell homeostasis in a number of mammalian tissues[1,2,4,14], we set out to study the role of *Bmi1* in the adult incisor.

To investigate *Bmi1* expression, we used $Bmi1^{GFP}$ reporter mice, in which the second exon of *Bmi1* was replaced by GFP, resulting in a null allele[15]. In $Bmi1^{GFP/+}$ adult mice, GFP was expressed in cells of the stellate reticulum and in the outer enamel epithelium (OEE), where the LaCL stem cells reside (Fig. 1a–c). These cells underwent infrequent cell divisions[12] and thus retained H2B–GFP or BrdU after extended chase periods (Figs 1b, 2f), similar to stem cells of the hair follicle bulge[16]. Furthermore, in $Bmi1^{GFP/+}$;$Gli1^{LacZ/+}$ mice, $Bmi1^{GFP}$ was co-expressed with $Gli1^{LacZ}$, a marker for adult dental stem cells[12] (Supplementary Fig. S1a–d). Together, these data suggested that *Bmi1* marks the incisor stem cells.

To determine whether *Bmi1*-expressing cells are indeed stem cells that can give rise to differentiated cell types over a long period of time, we performed inducible genetic lineage tracing. This technique permanently labels a cell and its progeny and definitively identifies adult stem cells *in vivo*[17]. To this end, we genetically labelled *Bmi1*-expressing cells and traced their descendants using an inducible $Bmi1^{CreER}$ strain[18] crossed to a Cre-responsive reporter line (*R26R-Tm–GFP*; ref. 19). Induction of Cre activity by tamoxifen injection results in permanent expression of GFP in *Bmi1*-expressing cells and their progeny. Whereas

[1]Department of Orofacial Sciences and Program in Craniofacial and Mesenchymal Biology, University of California San Francisco, San Francisco, California 94143, USA. [2]Department of Pediatrics and Institute for Human Genetics, University of California San Francisco, San Francisco, California 94143, USA. [3]Howard Hughes Medical Institute and Department of Human Genetics, University of Utah School of Medicine, Salt Lake City, Utah 84112, USA. [4]Smilow Neuroscience Program, Department of Physiology and Neuroscience, Howard Hughes Medical Institute, NYU School of Medicine, New York, USA. [5]Department of Preventative and Restorative Dental Sciences, University of California San Francisco, San Francisco, California 94143, USA. [6]These authors contributed equally to this work. [7]Present addresses: Department of Molecular Biology, Genentech Inc., 1 DNA Way, South San Francisco, California 94080, USA (B.B.); Istituto di Genetica Medica, Università Cattolica del Sacro Cuore, Rome, Italy (E.S.).
[8]Correspondence should be addressed to O.D.K. (e-mail: Ophir.Klein@ucsf.edu)

Received 12 June 2012; accepted 19 April 2013; published online 2 June 2013; DOI: 10.1038/ncb2766

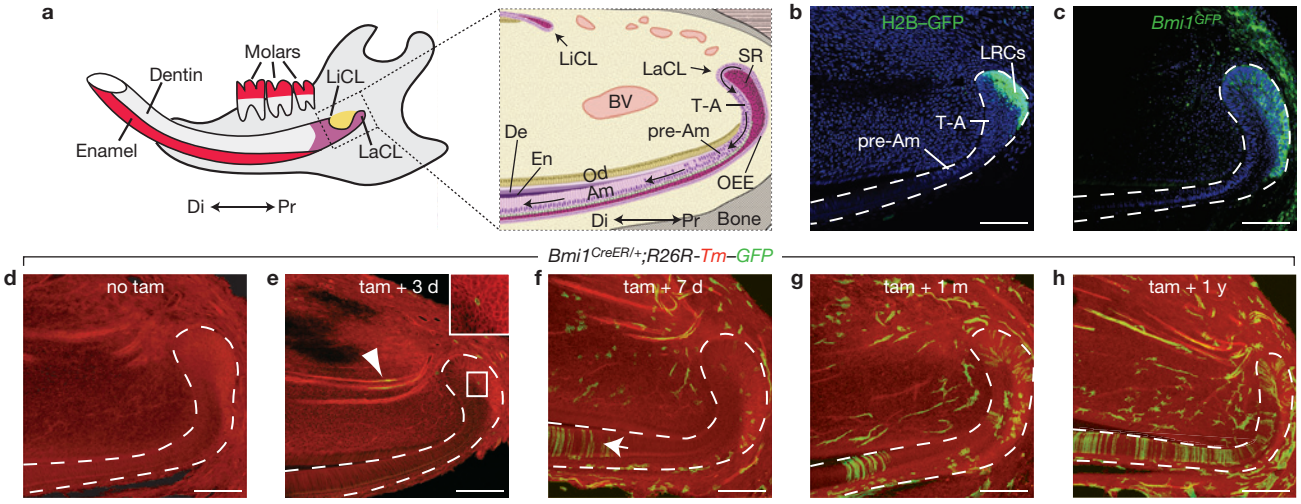

Figure 1 *Bmi1*-expressing cells in the dental epithelium are stem cells. (**a**) Left, schematic diagram of an adult mandible. The incisor is a long tooth that grows under the molars. Enamel is produced by ameloblasts, which are present only on the labial surface. Dentin, produced by odontoblasts, is deposited on both the labial and lingual surfaces. Di, distal; LiCL, lingual cervical loop; LaCL, labial cervical loop; Pr, proximal. Right, schematic representation of the cell types associated with the dental epithelium and stem cell niche. The arrows in the labial epithelium represent the direction of movement of the cells as they differentiate. Am, ameloblasts. BV, blood vessel; De, dentin; En, enamel; Od, odontoblasts. OEE; outer enamel epithelium; pre-AM, pre-ameloblasts; SR, stellate reticulum; T-A, transit amplifying. (**b**) *K5tTA;H2BGFP* mice treated for 2 months with doxycycline reveal label retention in the stellate reticulum and OEE of the LaCL. (**c**) $Bmi1^{GFP}$ expression is localized to the OEE and stellate reticulum of the cervical loop. (**d**–**h**) $Bmi1^{CreER}$*;R26R-Tm–GFP* mice were induced at 6 weeks with tamoxifen and chased for the indicated time period. The dashed lines in **b**–**h** outline the dental epithelium. Scale bars, 100 μm.

we did not detect GFP labelling in uninjected $Bmi1^{CreER/+;}$ *R26R-Tm–GFP* mice (Fig. 1d), we observed a few labelled cells in the LaCL and surrounding mesenchyme 3 days after tamoxifen injection (Fig. 1e, inset). GFP was also observed in blood vessels (Fig. 1e, arrowhead), consistent with a previous report of *Bmi1* expression in endothelium[20]. By 7 days after tamoxifen injection, increased numbers of GFP-positive cells were observed in the LaCL and mesenchyme (Fig. 1f). Importantly, as cells in the pre-ameloblast region move ~350 μm d^{-1} (refs 21,22), the appearance of GFP-positive pre-ameloblasts in the dental epithelium (Fig. 1f, arrow) several days after tamoxifen injection established the production of differentiated cells from *Bmi1*-positive progenitors. Longer chases revealed the accumulation of labelled cells in the LaCL, indicating that LaCL stem cells had undergone self-renewal (Fig. 1g,h). The appearance of groups of labelled ameloblasts suggested that each cluster represented the progeny of a single stem cell whose descendants underwent several rounds of replication. Together, the expression and lineage tracing data demonstrated that *Bmi1*-expressing cells in the LaCL are stem cells.

Next, to identify the function of *Bmi1* in the mouse incisor, we analysed the architecture of the dental epithelium in *Bmi1*-null animals ($Bmi1^{GFP/GFP}$, hereafter referred to as $Bmi1^{-/-}$), at 5 months of age by performing haematoxylin and eosin staining. $Bmi1^{-/-}$ animals had LaCLs that were consistently thinner in both the sagittal and coronal planes, with a substantial decrease in the amount of stellate reticulum compared with $Bmi1^{+/+}$ siblings (Fig. 2a,h). To obtain a clearer picture of the morphological defect in $Bmi1^{-/-}$ LaCLs, we prepared three-dimensional (3D) reconstructions of the LaCL from $Bmi1^{+/+}$ and $Bmi1^{-/-}$ animals. The 3D reconstructions demonstrated a significant loss of tissue in the LaCL, specifically in the stellate reticulum on the labial side (Fig. 2b,i, and Supplementary Fig. S2). On average, $Bmi1^{-/-}$ LaCLs showed a 28% decrease in total volume when compared with controls (Fig. 2v).

We then investigated whether the expression profile was altered in $Bmi1^{-/-}$ LaCLs by analysing markers of dental epithelium. E-cadherin is normally expressed in stem cells residing in the stellate reticulum and OEE and downregulated in the T-A zone[21] (Fig. 2c). Conversely, P-cadherin is absent in the stem cell region but upregulated in the T-A region[21] (Fig. 2e). In $Bmi1^{-/-}$ LaCLs, the domain of E-cadherin expression was smaller (Fig. 2j), and P-cadherin staining was expanded posteriorly into the OEE (Fig. 2l, asterisk), indicating that cells in this region assumed a more differentiated character. We next examined the expression of integrin alpha 6 (ITGA6), a marker of haematopoietic[23], neural[23], tracheal[24] and epidermal[25] stem cells that is also expressed in the dental epithelial stem cells[26]. Similarly to E-cadherin, ITGA6 is normally expressed in the stellate reticulum and OEE of the LaCL (Fig. 2d), and its domain of expression was markedly smaller in the LaCL of $Bmi1^{-/-}$ animals (Fig. 2k). Together, the expression pattern of these markers indicated that a loss of *Bmi1* activity caused a reduction in the size of the stem-cell-containing region in the incisor.

As *Bmi1* is known to regulate stem cell self-renewal[1,2,4], we examined whether the reduction of cells in the $Bmi1^{-/-}$ LaCLs was due at least in part to a reduced population of stem cells, using BrdU label retention as a marker of these cells[8,12]. We administered BrdU to perinatal $Bmi1^{+/+}$ and $Bmi1^{-/-}$ pups and analysed the number of label-retaining cells (LRCs) in 6-week-old adult mice (Fig. 2f,m). On average, $Bmi1^{-/-}$ LaCLs had 45% fewer LRCs when compared with $Bmi1^{+/+}$ controls (Fig. 2w), indicating that *Bmi1* regulates stem cell number in the incisor. However, there was no increase in apoptosis in the mutants.

Finally, as *Bmi1*-expressing stem cells give rise to enamel-secreting ameloblasts, we compared the mineralized enamel in $Bmi1^{+/+}$ and

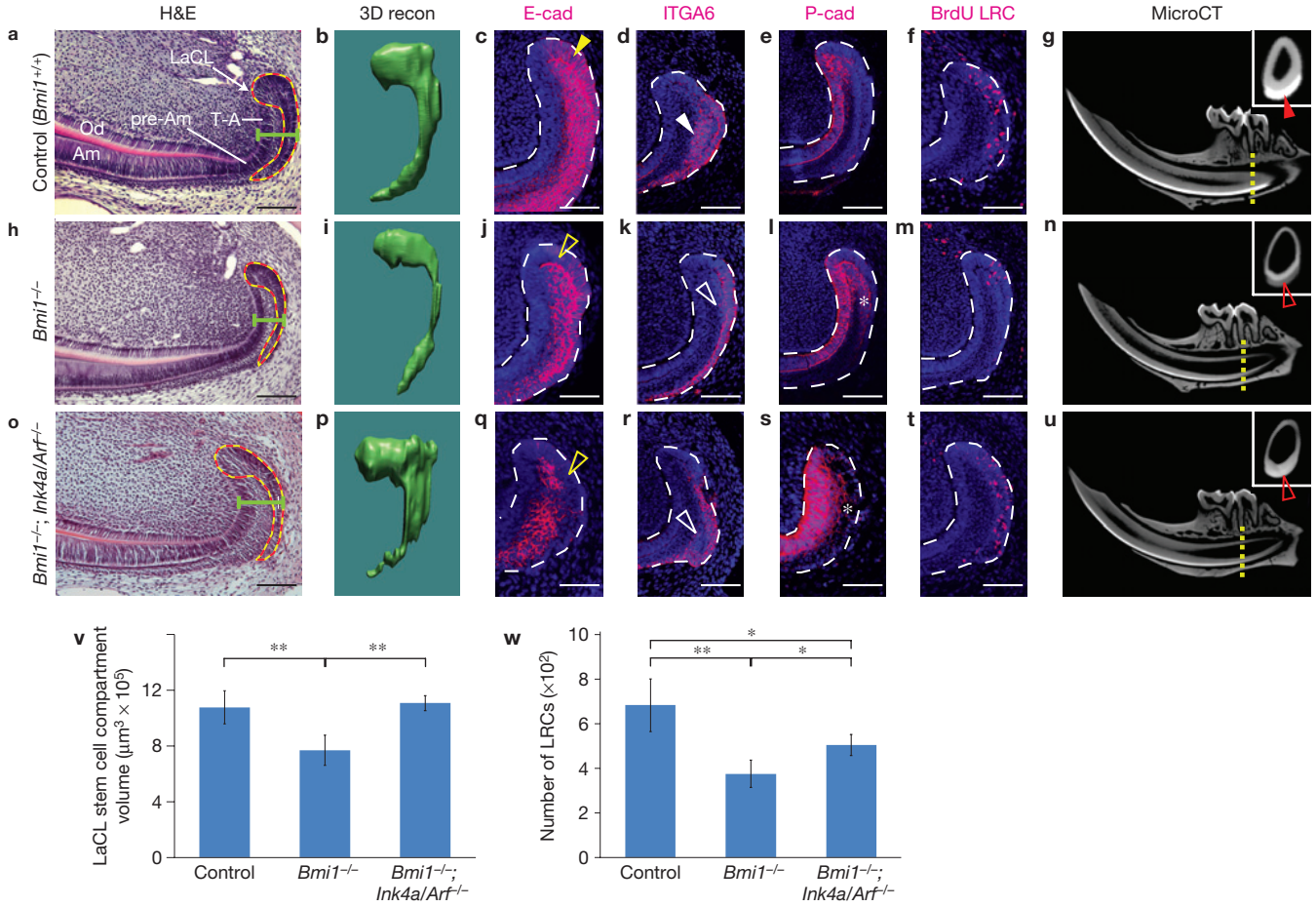

Figure 2 Deletion of *Bmi1* affects adult LaCL through both *Ink4a/Arf*-dependent and -independent mechanisms. (**a**,**h**,**o**) Haematoxylin and eosin (H&E) staining comparing LaCLs from 5-month-old control (*Bmi1*$^{+/+}$), *Bmi1*$^{-/-}$ and *Bmi1*$^{-/-}$;*Ink4a/Arf*$^{-/-}$ mice. The dashed lines outline the region traced on coronal sections for 3D renderings. The green bar demarcates the width of the cervical loop. (**b**,**i**,**p**) 3D renderings enable reconstruction (recon) of the control, *Bmi1*$^{-/-}$ and *Bmi1*$^{-/-}$;*Ink4a/Arf*$^{-/-}$ (triple mutant) LaCLs. (**c**,**j**,**q**) E-cadherin staining of the LaCL in control, *Bmi1* and triple mutants. E-cadherin expression is downregulated in both the single and triple mutants (open yellow arrowheads) when compared with the control (yellow arrowhead). (**d**,**k**,**r**) The expression level of ITGA6 detected by immunostaining is decreased in the *Bmi1*$^{-/-}$ and *Bmi1*$^{-/-}$;*Ink4a/Arf*$^{-/-}$ LaCLs (open white arrowheads) when compared with the control (white arrowhead). (**e**,**l**,**s**) P-cadherin expression in the LaCL is expanded in both the *Bmi1* and *Bmi1*$^{-/-}$;*Ink4a/Arf*$^{-/-}$ LaCLs (asterisks). (**f**,**m**,**t**) Representative sections of LaCLs from control, *Bmi1*$^{-/-}$ and *Bmi1*$^{-/-}$;*Ink4a/Arf*$^{-/-}$ jaws. Animals were pulsed with BrdU postnatally and aged 1.5 months for identification of LRCs. (**g**,**n**,**u**) MicroCT scans showing mandibles from 5-month-old control, *Bmi1*$^{-/-}$ and *Bmi1*$^{-/-}$;*Ink4a/Arf*$^{-/-}$ mice. Enamel is thinner and less mineralized in both single and triple mutants when compared with the control. Insets are coronal sections through the distal root of the second molar (yellow dotted lines) and show that enamel is less mineralized in mutants (open red arrowheads) than in the control (red arrowhead). (**v**) Quantification of the volume of the LaCL stem cell compartment in control, *Bmi1*$^{-/-}$ and *Bmi1*$^{-/-}$;*Ink4a/Arf*$^{-/-}$ mice ($n = 4$ mice for each genotype). (**w**) Quantification of BrdU LRCs by sectioning and staining through the entire LaCL ($n = 5$ control, 3 *Bmi1*$^{-/-}$, and 4 *Bmi1*$^{-/-}$;*Ink4a/Arf*$^{-/-}$ mice). Error bars indicate means ± s.d. $^{*}P < 0.05$, $^{**}P < 0.001$. Scale bars, 100 μm for **a**,**h**,**o**, and 75 μm for **c**–**f**, **j**–**m**, and **q**–**t**. Source data of statistical analyses are shown in Supplementary Tables S2 and S3.

Bmi1$^{-/-}$ lower incisors using microtomography scans (microCT). In 5-month-old *Bmi1*$^{+/+}$ adults, mature enamel was present in a swath that extended from a region proximal to the molars to the distal tip of the tooth (Fig. 2g). In contrast, mature *Bmi1*$^{-/-}$ enamel receded to a position between the proximal and distal roots of the first molar, indicating defective enamel formation by *Bmi1*$^{-/-}$ progeny (Fig. 2n).

In other contexts, BMI1 and other polycomb group proteins preserve stem cell self-renewal through repression of the *Ink4a/Arf* locus, which encodes two tumour-suppressor proteins that negatively regulate the cell cycle[1,3,4]. As *Ink4a/Arf* was also upregulated in the *Bmi1*-null incisor epithelium (Fig. 3a), it was possible that BMI1 functions similarly in mouse incisor stem cells by repressing *Ink4a/Arf* expression. To investigate this possibility and to dissect phenotypes associated with *Ink4a/Arf* upregulation, we bred *Bmi1*$^{-/-}$;*Ink4a/Arf*$^{-/-}$ triple mutants. We first observed that the deletion of *Ink4a/Arf* was able to restore LaCL volume (Fig. 2o,p,v). *Ink4a/Arf* deletion also partially rescued LRC number (Fig. 2t,w), consistent with the notion that *Bmi1* is required to maintain an adequate population of stem cells for homeostasis by repressing *Ink4a/Arf* expression. However, the incompleteness of the rescue pointed to the existence of other BMI1 targets that may contribute to the mutant phenotype. Similarly, in other organs, deletion of *Ink4a/Arf* in *Bmi1*-null animals was insufficient to completely rescue either the morphological defects[4] or the maintenance of downstream lineage specification[14]. Indeed, the marker expression pattern of the *Bmi1*$^{-/-}$;*Ink4a/Arf*$^{-/-}$ mutant LaCL resembled that of the *Bmi1*-null incisor, with diminished E-cadherin and ITGA6 expression in the stellate

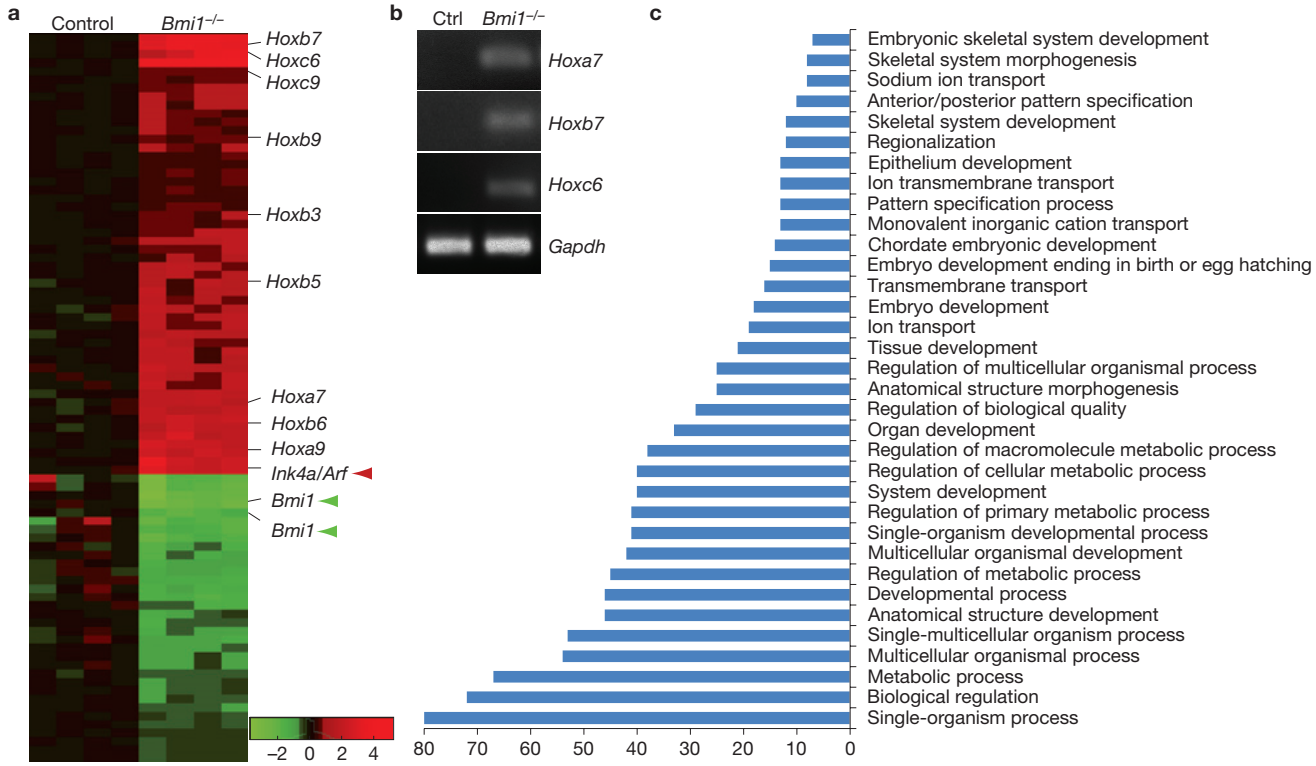

Figure 3 *Bmi1* suppresses expression of *Ink4a/Arf* and *Hox* genes. (**a**) Microarray analysis on $Bmi1^{+/+}$ (control or ctrl) and $Bmi1^{-/-}$ dental epithelia shows that inactivation of *Bmi1* leads to de-regulation of *Ink4a/Arf* (red arrowhead), as well as several *Hox* genes. Loss of *Bmi1* expression is indicated by green arrowheads. (**b**) PCR with reverse transcription analysis showing upregulation of *Hoxa7, b7,* and *c*6 in $Bmi1^{-/-}$ LaCLs. (**c**) Gene ontology analysis reveals upregulation of genes normally involved in developmental processes and cell differentiation.

reticulum and OEE, accompanied by an expanded P-cadherin domain (Fig. 2q–s), suggesting that *Bmi1* maintains incisor stem cell identity through mechanisms that do not involve *Ink4a/Arf*. Importantly, despite the rescue in LaCL size, $Bmi1^{-/-}$;$Ink4a/Arf^{-/-}$ mice exhibited defects in enamel deposition (Fig. 2u), a phenotype that is probably due to abnormal gene expression in stem cells and their progeny.

To identify other BMI1 targets, we performed microarray analysis on dental epithelia from control and *Bmi1*-null incisors. Besides *Ink4a/Arf*, many other genes were upregulated in the mutants, including 9 *Hox* genes from 3 different *Hox* clusters (Fig. 3a). To validate the upregulation of *Hox* genes in *Bmi1*-null dental epithelia, we performed PCR with reverse transcription on $Bmi1^{+/+}$ and $Bmi1^{-/-}$ LaCLs. Whereas *Hoxa7*, *b7* and *c*6 transcripts were undetectable in control LaCLs, their expression was readily detected in $Bmi1^{-/-}$ LaCLs (Fig. 3b). Similarly, *Hoxc9* and *a*9 expression was markedly increased in the $Bmi1^{-/-}$ LaCLs. Thus, BMI1 suppressed the expression of several *Hox* genes in the LaCL, suggesting that de-repressed *Hox* transcription may lead to premature differentiation. Gene ontology analysis further confirmed this notion, as genes associated with differentiation were upregulated in the mutants (Fig. 3c and Supplementary Table S1). Specifically, genes important for enamel formation that are normally expressed in maturing ameloblasts, such as *Amelotin* (*Amtn*) and *Kallikrein-related peptidase* (*Klk4*; refs 27,28), were prematurely upregulated in the LaCL (Supplementary Table S1).

It was next important to determine whether BMI1-mediated repression of *Hox* genes was functionally required for the regulation of adult incisor stem cells. We used a tissue culture system[21,29] to enable concurrent manipulation of *Hox* expression levels in incisor stem cells. LaCL epithelia from $Bmi1^{+/+}$ or $Bmi1^{-/-}$ incisors were dissociated to create single-cell suspensions. Ten days after plating control cells, three morphological types of colony appeared, with most colonies being composed of small and tightly packed cells that continued to express E-cadherin, suggesting that they maintained some of the incisor stem cell characteristics (Supplementary Fig. S3a–g). In contrast, dissociated LaCL cells from $Bmi1^{-/-}$ incisors grew very poorly and produced far fewer colonies (Supplementary Fig. S3h), consistent with upregulation of *Ink4a/Arf* and the self-renewal defects described above, but no change in apoptosis was observed in cultured $Bmi1^{-/-}$ cells (Supplementary Fig. S1g,h). Finally, sorting of cells from $Bmi1^{GFP/+}$ animals showed that cells with a higher GFP expression level (GFP^{HI}) produced significantly more colonies than cells with low GFP (GFP^{LO}; Supplementary Fig. S3i,j). Together, these data supported the functional results and confirmed that *Bmi1* is required to maintain dental epithelial stem cells.

We then tested whether *Ink4a/Arf* deletion could rescue the colony-forming defect associated with loss of *Bmi1* activity by culturing LaCL cells from $Bmi1^{-/-}$;$Ink4a/Arf^{-/-}$ mice. In contrast to the *Bmi1* mutants, the dissociated $Bmi1^{-/-}$;$Ink4a/Arf^{-/-}$ LaCL cells readily formed colonies that were comparable in numbers to the control (Supplementary Fig. S3h); however, the $Bmi1^{-/-}$;$Ink4a/Arf^{-/-}$ colonies contained larger cells (Fig. 4a,b). We reasoned that whereas $Bmi1^{-/-}$ cells normally cannot self-renew owing to elevated *Ink4a/Arf* expression level, deletion of the *Ink4a/Arf* locus enabled these cells to proliferate. The altered morphology in $Bmi1^{-/-}$;$Ink4a/Arf^{-/-}$ cells suggested that

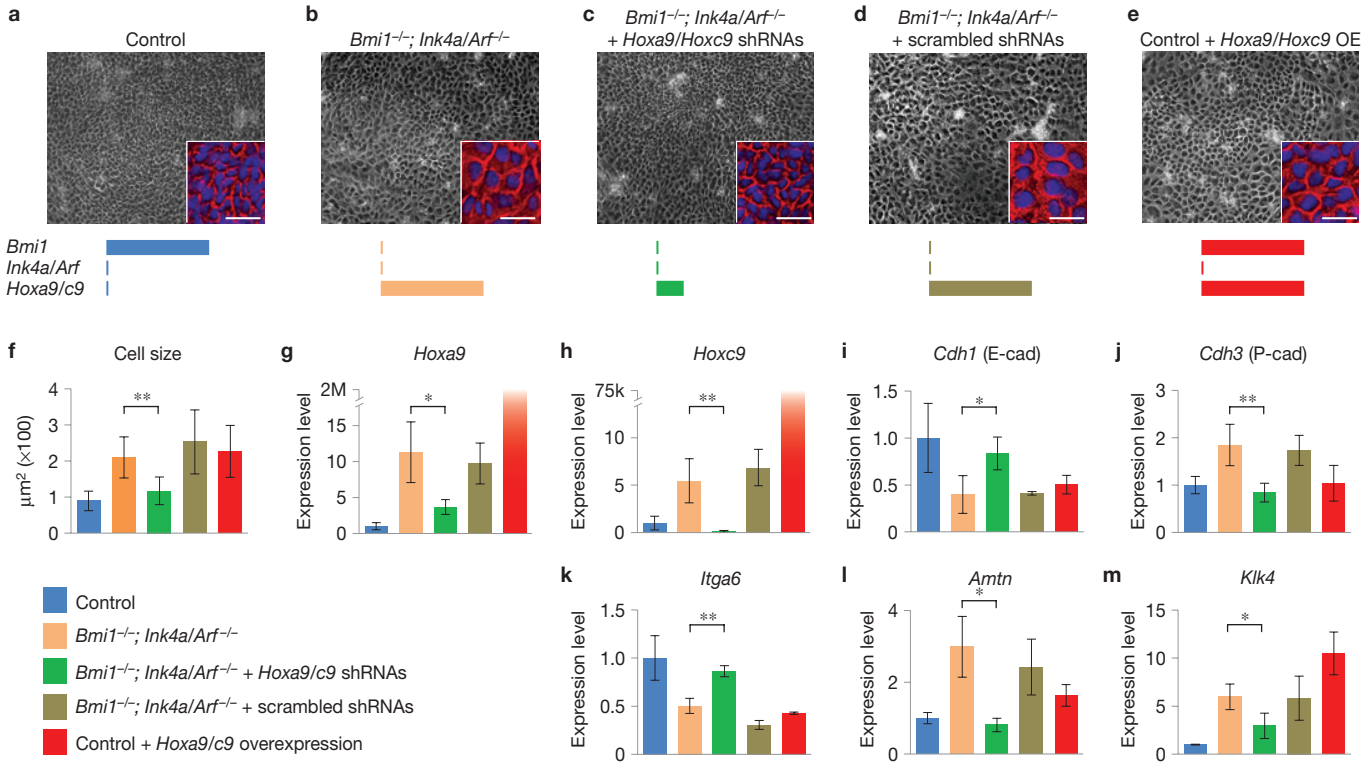

Figure 4 *Hox* gene upregulation contributes to the *Bmi1* loss-of-function phenotype. (**a**) Stem cell colonies derived from control LaCLs are composed of small, rounded cells. (**b**) Deletion of *Ink4a/Arf* enables colony formation by $Bmi1^{-/-}$ cells, but the cell size is increased. (**c**) Knockdown of *Hoxa9* and *Hoxc9* rescues the morphological defects in $Bmi1^{-/-}$; $Ink4a/Arf^{-/-}$ colonies. (**d**) Scrambled shRNA does not rescue the phenotype. (**e**) Overexpression (OE) of *Hoxa9* and *Hoxc9* in control cells phenocopies the morphology of $Bmi1^{-/-}$; $Ink4a/Arf^{-/-}$ colonies. The insets in **a**–**e** are enlarged images of representative cells with a pseudo-coloured cell boundary (red) and DAPI nuclear staining (blue). Schematics represent the level of expression for each gene. (**f**) Quantification of cell size under different conditions ($n = 3$ independent experiments with 100 cells scored for each experiment). (**g**–**m**) Relative expression level by qPCR of *Hoxa9*, *Hoxc9*, *Cdh1*, *Cdh3*, *Itga6*, *Amtn* and *Klk4* in cells cultured under different conditions ($n = 3$ independent experiments). Error bars indicate means ± s.d. $^{*}P < 0.05$, $^{**}P < 0.001$. Scale bars, 100 µm (**a**–**e**) and 30 µm (insets). Source data of statistical analyses are shown in Supplementary Tables S4 and S5.

BMI1 also regulates a developmental program that is independent of *Ink4a/Arf* expression. Consistent with this notion, the transcriptomes of $Bmi1^{-/-}$;$Ink4a/Arf^{-/-}$ colonies were markedly different from wild-type controls and very similar to $Bmi1^{-/-}$ colonies (Supplementary Fig. S4). Thus, BMI1 must control cell morphology and differentiation by regulating the expression of other genes.

To determine whether upregulation of *Hox* genes was an important contributor to the mutant phenotype in *Bmi1*-null incisors, we used lentiviral transduction to introduce short hairpin RNAs (shRNAs) against *Hoxa9* and *Hoxc9*. These genes were the most upregulated *Hox* family members in both $Bmi1^{-/-}$ and $Bmi1^{-/-}$;$Ink4a/Arf^{-/-}$ mutants, as well as in colonies derived from these animals (Figs 3a, 4g,h). Quantitative PCR (qPCR) results demonstrated that the shRNAs effectively knocked down *Hoxa9* and *Hoxc9*, whereas control scrambled sequences did not (Fig. 4g,h). Furthermore, the doubly infected colonies exhibited morphology and cell size similar to controls (Fig. 4a,c,f). The rescue by *Hoxa9/c9* shRNAs coincided with upregulation of *Cdh1* (encoding E-cadherin) and *Itga6* and with downregulation of *Cdh3* (encoding P-cadherin), *Amtn* and *Klk4* (Fig. 4i–m, Supplementary Fig. S5c–g), although single knockdown of either *Hox* gene alone did not show a clear rescue (Supplementary Fig. S5h,i), most likely owing to functional redundancy. Thus, reducing the level of *Hoxa9/c9* expression reconstituted the incisor epithelial stem cell expression signature, which indicated that deregulated expression of *Hoxa9* and *Hoxc9* was at least partially responsible for the changes in stem cell morphology and gene expression in $Bmi1^{-/-}$ cells.

Repression of *Hox* genes in the adult dental stem cells is therefore an important function of *Bmi1*, and this finding led us to predict that overexpression of *Hox* genes in the LaCL would phenocopy the $Bmi1^{-/-}$ mutants. To that end, we first introduced exogenous *Hoxa9/c9* by lentiviral transduction into cultured control LaCL cells (Fig. 4e,g,h). This overexpression caused enlarged cell size, downregulated expression of *Cdh1* and *Itga6*, and upregulated *Amtn* and *Klk4* expression, all of which are characteristic of the $Bmi1^{-/-}$ mutants (Fig. 4f,i–m). However, the level of *Cdh3* expression was not altered, suggesting that other genes and/or factors were required for its upregulation. To further test whether *Hox* genes function similarly *in vivo*, we generated $Gli1^{CreER/+}$;$R26^{Hoxc9/YFP}$ mice, in which ectopic *Hoxc9* expression and a YFP Cre-reporter were induced specifically in the LaCL stem cells by tamoxifen injection (Fig. 5a,f). Overexpression of *Hoxc9* led to downregulation of E-cadherin and ITGA6 in the stellate reticulum and OEE and to expanded P-cadherin expression (Fig. 5b–d,g–i), matching the gene expression phenotype exhibited by the $Bmi1^{-/-}$ mutants, although LaCL size was not affected (Fig. 5e,j,k).

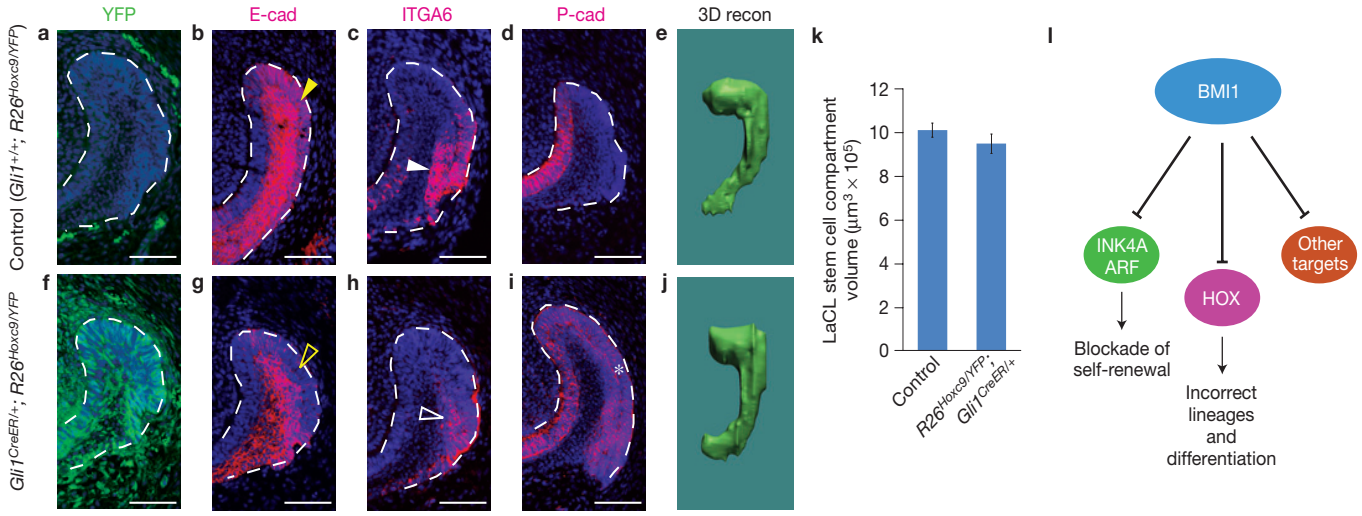

Figure 5 Overexpression of *Hoxc9* in LaCLs phenocopies *Bmi1* mutants. (**a**,**f**) *Hoxc9* and YFP Cre-reporter were overexpressed using a $Gli1^{CreER}$ driver in the LaCL by tamoxifen induction, but not in the absence of Cre. YFP expression is shown here 10 days after induction. (**b**,**g**) E-cadherin is expressed in stellate reticulum and OEE in the control LaCL (yellow arrowhead) but downregulated in the mutant (open yellow arrowhead). (**c**,**h**) ITGA6 is similarly downregulated in the mutant (compare solid and open white arrowheads). (**d**,**i**) P-cadherin expression is restricted in the T-A region in the control but expanded in the mutant (asterisk). All LaCLs are outlined by white dashed lines. Scale bar, 75 μm. (**e**,**j**,**k**) 3D reconstruction (recon) of LaCLs shows no difference in LaCL size between control and $Gli1^{CreER/+}$; $R26^{Hoxc9/YFP}$ ($n = 3$ animals for each genotype). Error bars indicate means ± s.d. Source data of statistical analysis are shown in Supplementary Table S2. (**l**) Model for function of BMI1 in incisor stem cells.

Together, these data demonstrate that *Bmi1*-positive cells in the LaCL are adult stem cells and that *Bmi1* function is required to maintain these cells through two distinct mechanisms (Fig. 5l). The first is through repression of *Ink4a/Arf* expression to permit stem cell self-renewal, a well-documented function of *Bmi1* in other systems[1,3,4]. However, the $Bmi1^{-/-}$ phenotype was not fully rescued by the deletion of *Ink4a/Arf*, and thus, prevention of arrested cell division is not the sole function of BMI1. We found that the second function of BMI1 is to suppress the expression of *Hox* genes to prevent inappropriate cell differentiation. A similar observation was made in the *Drosophila* testis, where mutated polycomb genes resulted in *Abdominal-B* upregulation and abnormal cyst stem cell differentiation[30], hinting at an evolutionarily conserved role for *Bmi1* in regulating stem cell differentiation. It is notable that upregulation of *Hox* genes has also been documented in other $Bmi1^{-/-}$ adult stem cells[1,2,5–7], and it will be important to consider the role of repression of *Hox* genes and other targets by BMI1 in those systems. For example, in haematopoietic stem cells, *Ebf1* and *Pax5* (ref. 14) regulate lineage specification, and their upregulation in *Bmi1* mutants causes a lineage shift during haematopoiesis. In the *Bmi1*-null incisor, we observed upregulation of genes associated with maturing ameloblasts as well as upregulation of *Hox* genes, which is probably the cause of the abnormal enamel deposition by $Bmi1^{-/-}$ ameloblasts. Thus, we propose that *Bmi1* has two distinct functions: maintain adequate stem cell self-renewal by suppressing *Ink4a/Arf*; and prevent inappropriate differentiation by inhibiting the expression of *Hox* genes and other genes important for cellular maturation (Fig. 5i). □

METHODS

Methods and any associated references are available in the online version of the paper.

Note: Supplementary Information is available in the online version of the paper

ACKNOWLEDGEMENTS

We thank members of the Klein laboratory for helpful advice, F. Michon for discussion, D-K. Tran and S. Alto for technical assistance, X-P. Wang for help with the culture system, A. Barczak and the UCSF Microarray Core Facilities for help with experiments and analysis, and Irving Weissman for mice. This work was supported by R01-DE021420 (NIH/NIDCR) and a CIRM New Faculty Award II, both to O.D.K.

AUTHOR CONTRIBUTIONS

B.B., J.K-H.H., N.B.S., H.J., E.S., R-P.H., A.F.G., J.S.D and O.D.K. designed and performed experiments. B.B., J.K-H.H and O.D.K. wrote the manuscript. All authors discussed results, analysed data and edited the manuscript.

COMPETING FINANCIAL INTERESTS

The authors declare no competing financial interests.

Published online at www.nature.com/doifinder/10.1038/ncb2766
Reprints and permissions information is available online at www.nature.com/reprints

1. Molofsky, A. V. *et al.* Bmi-1 dependence distinguishes neural stem cell self-renewal from progenitor proliferation. *Nature* **425,** 962–967 (2003).
2. Park, I. K. *et al.* Bmi-1 is required for maintenance of adult self-renewing haematopoietic stem cells. *Nature* **423,** 302–305 (2003).
3. Jacobs, J. J., Kieboom, K., Marino, S., DePinho, R. A. & van Lohuizen, M. The oncogene and Polycomb-group gene bmi-1 regulates cell proliferation and senescence through the ink4a locus. *Nature* **397,** 164–168 (1999).
4. Molofsky, A. V., He, S., Bydon, M., Morrison, S. J. & Pardal, R. Bmi-1 promotes neural stem cell self-renewal and neural development but not mouse growth and survival by repressing the p16Ink4a and p19Arf senescence pathways. *Genes Dev.* **19,** 1432–1437 (2005).
5. Zacharek, S. J. *et al.* Lung stem cell self-renewal relies on BMI1-dependent control of expression at imprinted loci. *Cell Stem Cell* **9,** 272–281 (2011).
6. Bruggeman, S. W., Hulsman, D. & van Lohuizen, M. Bmi1 deficient neural stem cells have increased integrin dependent adhesion to self-secreted matrix. *Biochim. Biophys. Acta* **1790,** 351–360 (2009).
7. Fasano, C. A. *et al.* shRNA knockdown of Bmi-1 reveals a critical role for p21-Rb pathway in NSC self-renewal during development. *Cell Stem Cell* **1,** 87–99 (2007).
8. Harada, H. *et al.* Localization of putative stem cells in dental epithelium and their association with Notch and FGF signaling. *J. Cell Biol.* **147,** 105–120 (1999).
9. Wang, X. P. *et al.* An integrated gene regulatory network controls stem cell proliferation in teeth. *PLoS Biol.* **5,** 1324–1333 (2007).
10. Klein, O. D. *et al.* An FGF signaling loop sustains the generation of differentiated progeny from stem cells in mouse incisors. *Development* **135,** 377–385 (2008).

11. Smith, C. E. & Warshawsky, H. Cellular renewal in the enamel organ and the odontoblast layer of the rat incisor as followed by radioautography using 3H-thymidine. *Anat. Rec.* **183,** 523–561 (1975).
12. Seidel, K. *et al.* Hedgehog signaling regulates the generation of ameloblast progenitors in the continuously growing mouse incisor. *Development* **137,** 3753–3761 (2010).
13. Juuri, E. *et al.* Sox2+ stem cells contribute to all epithelial lineages of the tooth via Sfrp5+ progenitors. *Dev. Cell* **23,** 317–328 (2012).
14. Oguro, H. *et al.* Poised lineage specification in multipotential hematopoietic stem and progenitor cells by the polycomb protein Bmi1. *Cell Stem Cell* **6,** 279–286 (2010).
15. Hosen, N. *et al.* Bmi-1-green fluorescent protein-knock-in mice reveal the dynamic regulation of bmi-1 expression in normal and leukemic hematopoietic cells. *Stem Cells* **25,** 1635–1644 (2007).
16. Tumbar, T. *et al.* Defining the epithelial stem cell niche in skin. *Science* **303,** 359–363 (2004).
17. Joyner, A. L. & Zervas, M. Genetic inducible fate mapping in mouse: establishing genetic lineages and defining genetic neuroanatomy in the nervous system. *Dev. Dyn.* **235,** 2376–2385 (2006).
18. Sangiorgi, E. & Capecchi, M. R. Bmi1 is expressed *in vivo* in intestinal stem cells. *Nat. Genet.* **40,** 915–920 (2008).
19. Muzumdar, M. D., Tasic, B., Miyamichi, K., Li, L. & Luo, L. A global double-fluorescent Cre reporter mouse. *Genesis* **45,** 593–605 (2007).
20. Sangiorgi, E. & Capecchi, M. R. Bmi1 lineage tracing identifies a self-renewing pancreatic acinar cell subpopulation capable of maintaining pancreatic organ homeostasis. *Proc. Natl Acad. Sci. USA* **106,** 7101–7106 (2009).
21. Li, C. Y. *et al.* E-cadherin regulates the behavior and fate of epithelial stem cells and their progeny in the mouse incisor. *Dev. Biol.* **366,** 357–366 (2012).
22. Hwang, W. S. & Tonna, E. A. Autoradiographic analysis of labeling indices and migration rates of cellular component of mouse incisors using tritiated thymidine (H3tdr). *J. Dent. Res.* **44,** 42–53 (1965).
23. Ramalho-Santos, M., Yoon, S., Matsuzaki, Y., Mulligan, R. C. & Melton, D. A. 'Stemness': transcriptional profiling of embryonic and adult stem cells. *Science* **298,** 597–600 (2002).
24. Rock, J. R. *et al.* Basal cells as stem cells of the mouse trachea and human airway epithelium. *Proc. Natl Acad. Sci. USA* **106,** 12771–12775 (2009).
25. Tani, H., Morris, R. J. & Kaur, P. Enrichment for murine keratinocyte stem cells based on cell surface phenotype. *Proc. Natl Acad. Sci. USA* **97,** 10960–10965 (2000).
26. Xiong, J., Mrozik, K., Gronthos, S. & Bartold, P. M. Epithelial cell rests of malassez contain unique stem cell populations capable of undergoing epithelial-mesenchymal transition. *Stem Cells Dev.* **21,** 2012–2025 (2012).
27. Simmer, J. P., Richardson, A. S., Smith, C. E., Hu, Y. & Hu, J. C. Expression of kallikrein-related peptidase 4 in dental and non-dental tissues. *Eur. J. Oral Sci.* **119,** 226–233 (2011).
28. Iwasaki, K. *et al.* Amelotin–a novel secreted, ameloblast-specific protein. *J. Dental Res.* **84,** 1127–1132 (2005).
29. Chavez, M. G. *et al.* Characterization of dental epithelial stem cells from the mouse incisor with two-dimensional and three-dimensional platforms. *Tissue Eng. C* **19,** 15–24 (2013).
30. Morillo Prado, J. R., Chen, X. & Fuller, M. T. Polycomb group genes Psc and Su(z)2 maintain somatic stem cell identity and activity in Drosophila. *PloS ONE* **7,** e52892 (2012).

METHODS

Mouse lines and injections. Mice carrying the *Bmi1*^{GFP} (ref. 15), *Bmi1*^{CreER} (ref. 18), *Gli1*^{CreER} (ref. 31), *Gli1*^{lacZ} (ref. 32), *K5tTA* (ref. 33), *R26R-Tm–GFP* (ref. 19), and *H2B–GFP* (ref. 16) alleles or transgenes were maintained and genotyped as previously described. For *R26*$^{Hoxc9/+}$, chicken (*Gallus gallus*) *Hoxc9* was cloned and inserted into the ROSA locus as described previously[34,35]. PCR genotyping for the *R26*^{Hoxc9} allele was performed using the following primers: R26wt_FW, 5′-AAAGTCGCTCTGAGTTGTTAT-3′; R26wt_REV, 5′-GGAGCGGGAGAAATGGATATG-3′; and R26loxC9_REV, 5′-GTTATGTAACGCGGAACTCCA-3′. *Gli1*^{CreER};*R26*$^{Hoxc9/YFP}$ mice were subsequently generated by mating *Gli1*$^{CreER/+}$;*R26*$^{YFP/+}$ male to *R26*$^{Hoxc9/Hoxc9}$ females. For lineage-tracing studies, 5 mg tamoxifen dissolved in corn oil was injected intraperitoneally into adult mice between 8 and 12 weeks of age at 5 mg per 25 g body weight. For label-retention studies, postnatal day-2 animals were injected with 200 µg BrdU for 3 consecutive days and euthanized after 6 weeks. At least three mice were examined at each time point for all experiments. Unless specified in the main text, 6-week-old mice were used. Both male and female mice were included in this study.

Lentiviral production and colony-forming assay. All shRNAs were designed using pSicoOligomaker 1.5 and cloned into the pSicoR–GFP vector (Tyler Jacks laboratory protocols, http://web.mit.edu/jacks-lab/protocols_table.html). Two sets of shRNAs against *Hoxa9* and *Hoxc9* were designed. The antisense sequences are: *Hoxa9* (first set), 5′-TTAATGCCATAAGGCCGGC-3′; *Hoxa9* scrambled (first set), 5′-TACTATCGGTAACGGACGC-3′; *Hoxa9* (second set), 5′-TAAACAGAAACTCCTTCTC-3′; *Hoxa9* scrambled (second set), 5′-AGTCTACAACTATTCACAC-3′; *Hoxc9* (first set), 5′-ATTGAAGAGAAACTCCTTC-3′; *Hoxc9* scrambled (first set), 5′-ACATGAATTAAGTTCCGAC-3′; *Hoxc9* (second set), 5′-ATAGACCACAGACGACTGC-3′; *Hoxc9* scrambled (second set), 5′-ACGTACGAGAAACAGCTCC-3′. Lentiviral packaging was performed using a third- generation packaging system (Addgene) according to established protocols. The *in vitro* culture system was modelled after a system for culture of hair follicle stem cells[36–38] and has been previously published[29]. Briefly, whole incisors, including the entire dental epithelium, were isolated from mandibles and incubated in collagenase (Worthington) for 4 h on ice. LaCLs were mechanically isolated and dissociated in 100 µl Accumax (Sigma) at 37 °C for 1 h using gentle pipetting. Cells were counted and plated at a density of 15,000 cells per well on a 6-well plate. Colonies were then either collected for RNA extraction or counted and imaged on a Leica inverted microscope after 10 days. All experiments were performed at least three times. Colony-forming efficiency was expressed as a ratio of the number of small-cell-containing colonies divided by the total number of plated cells. Cell sizes were measured using ImageJ ($n = 3$ independent experiments, and 100 cells were scored for each experiment).

Flow cytometry. LaCLs from *Bmi1*$^{GFP/+}$ and *Bmi1*$^{+/+}$ mice were isolated and dissociated as described above. Single-cell suspensions were sorted for GFP expression using a FACSAria 2 cell sorter (BD Biosciences) at the Eli and Edythe Broad Center of Regeneration Medicine and Stem Cell Research at UCSF, Cell Analysis core. Two separate experiments were performed.

3D reconstruction of cervical loops. The epithelium was outlined from ∼40 consecutive 7-µm-thick coronal sections at the most proximal end of the mouse incisor ($n = 4$ animals per genotype). BioVis software (http://www.biovis3d.com) was used to generate 3D reconstructions from this data and to calculate the volume of the structures.

Microarray analysis and qPCR. Total RNA from dissected whole LaCLs or colonies was extracted using the Ambion Mirvana RNA Isolation kit. Sample preparation, labelling and array hybridizations were performed according to standard protocols from the UCSF Shared Microarray Core Facilities and Agilent Technologies (http://www.arrays.ucsf.edu and http://www.agilent.com). Total RNA quality was assessed using a Pico Chip on an Agilent 2100 Bioanalyzer (Agilent Technologies). The data sets were normalized using the quantile normalization method[39]. No background subtraction was performed, and the median feature pixel intensity was used as the raw signal before normalization. A one-way analysis of variance linear model was fitted to the comparison to estimate the mean M values and calculate moderated t-statistic, B statistic, false discovery rate, and P value for each gene for the comparison of interest. All procedures were carried out using functions in the R package limma in Bioconductor. Gene ontology analysis was performed using the Term Enrichment tool in AmiGO (http://amigo.geneontology.org). For qPCR analysis, complementary DNA was generated using the Advantage RT for PCR kit (Clontech), and TaqMan assays (Ambion) were used to perform qPCR. Primers for *Hoxc9*, *Amtn*, *Klk4* and *L19* were ordered from IDT PrimeTime. Primer sequences for *Hoxa9*, *Cdh1*, *Cdh3* and *Itga6* are: *Hoxa9* forward, 5′-GAATGAGAGCGGCGGAGAC-3′, reverse, 5′-GAGCGAGCATGTAGCCAGTTG-3′; *Cdh1*, forward, 5′-AATGAAGCCCCCATCTTTAT-3′, reverse, 5′-GAGATGGA-CAGAGAAGACGC-3′; *Cdh3*, forward, 5′-CCGCATCTTAAGGAGACGAA-3′, reverse 5′-AAATCTTGGTGCCTCTGTCC-3′; *Itga6*, forward, 5′-GGAGCCTCTT-CGGCTTCTC-3′, reverse, 5′-AGTGCTTCTGCCCGAGGT-3′. All samples were normalized to L19. CT values were extracted, and relative gene expression levels were calculated using the ΔΔCT method. All experiments were performed at least three times.

Histology and immunofluorescence microscopy. Jaws were dissected from perfusion-fixed animals, post-fixed in 4% PFA overnight, decalcified in RNase-free 0.5 M EDTA for 16 days, and processed for paraffin embedding. Sections (7 µm) were prepared and stained with haematoxylin and eosin using standard methods. For all images shown, representative samples were chosen after sectioning through the entire jaw, to avoid plane of section artefacts. Brightfield images were obtained using a Leica DFC 500 camera with a Leica DM 5000B microscope. For immunostaining, paraffin sections were rehydrated, incubated in 1 mM EDTA just below boiling temperature for 30 min for antigen retrieval, washed in distilled H_2O, and treated for 20 min with 3% H_2O_2 in PBS. Primary antibodies against GFP (1:5,000, Torrey Pines, TP401), E-cadherin (1:1,000, Invitrogen,131900), P-cadherin (1:1,000, Invitrogen, 132000Z), BrdU (1:500, Abcam, ab6326) and ITGA6 (1:1,000, Santa Cruz, sc-10730) were used. Washes in PBS (3 × 20 min) and PBS-T (1 × 5 min) were followed by incubation with Alexa Fluor 488 and 555 secondary antibodies (1:500, Invitrogen) or biotinylated anti-rat secondary antibody (Vector BA-4001) followed by signal amplification (Perkin Elmer). Sections were counterstained with DAPI (Vector Laboratories) and mounted in 1% DABCO in glycerol. Images were acquired using a Leica-TCS SP5 confocal microscope. BrdU staining was quantified using ImageJ. TUNEL staining was performed according to the manufacturer's protocol (Roche 12156792910). All experiments were performed at least three times.

MicroCT analysis. Hemimandibles ($n = 3$ per genotype) were imaged under wet conditions using a Micro XCT (Xradia, Pleasanton) at a ×2 magnification using a tungsten anode setting of 90 keV and 66 microamps. Virtual sections from reconstructed tomographs were used to study the X-ray attenuation of incisor enamel across groups under identical experimental parameters and at similar sectioning planes.

Statistical analysis. For statistical analyses, mean values with standard deviation (s.d.) are shown in most graphs. All experiments were performed independently at least three times, and the exact n numbers are listed in the figure legends. P values were obtained from Student's t-tests with paired samples. $P < 0.05$ was determined to be significant for all experiments. Actual P values are shown in each figure or figure legend.

Accession codes. Gene Expression Omnibus: GSE46001.

31. Ahn, S. & Joyner, A. L. Dynamic changes in the response of cells to positive hedgehog signaling during mouse limb patterning. *Cell* **118,** 505–516 (2004).
32. Bai, C. B., Auerbach, W., Lee, J. S., Stephen, D. & Joyner, A. L. Gli2, but not Gli1, is required for initial Shh signaling and ectopic activation of the Shh pathway. *Development* **129,** 4753–4761 (2002).
33. Diamond, I., Owolabi, T., Marco, M., Lam, C. & Glick, A. Conditional gene expression in the epidermis of transgenic mice using the tetracycline-regulated transactivators tTA and rTA linked to the keratin 5 promoter. *J. Invest. Dermatol.* **115,** 788–794 (2000).
34. Sousa, V. H., Miyoshi, G., Hjerling-Leffler, J., Karayannis, T. & Fishell, G. Characterization of Nkx6-2-derived neocortical interneuron lineages. *Cereb. Cortex* **19,** i1-10 (2009).
35. Jung, H. *et al.* Global control of motor neuron topography mediated by the repressive actions of a single hox gene. *Neuron* **67,** 781–796 (2010).
36. Rochat, A., Kobayashi, K. & Barrandon, Y. Location of stem cells of human hair follicles by clonal analysis. *Cell* **76,** 1063–1073 (1994).
37. Blanpain, C., Lowry, W. E., Geoghegan, A., Polak, L. & Fuchs, E. Self-renewal, multipotency, and the existence of two cell populations within an epithelial stem cell niche. *Cell* **118,** 635–648 (2004).
38. Barrandon, Y. & Green, H. Three clonal types of keratinocyte with different capacities for multiplication. *Proc. Natl Acad. Sci. USA* **84,** 2302–2306 (1987).
39. Bolstad, B. M., Irizarry, R. A., Astrand, M. & Speed, T. P. A comparison of normalization methods for high density oligonucleotide array data based on variance and bias. *Bioinformatics* **19,** 185–193 (2003).

DOI: 10.1038/ncb2766

nature cell biology

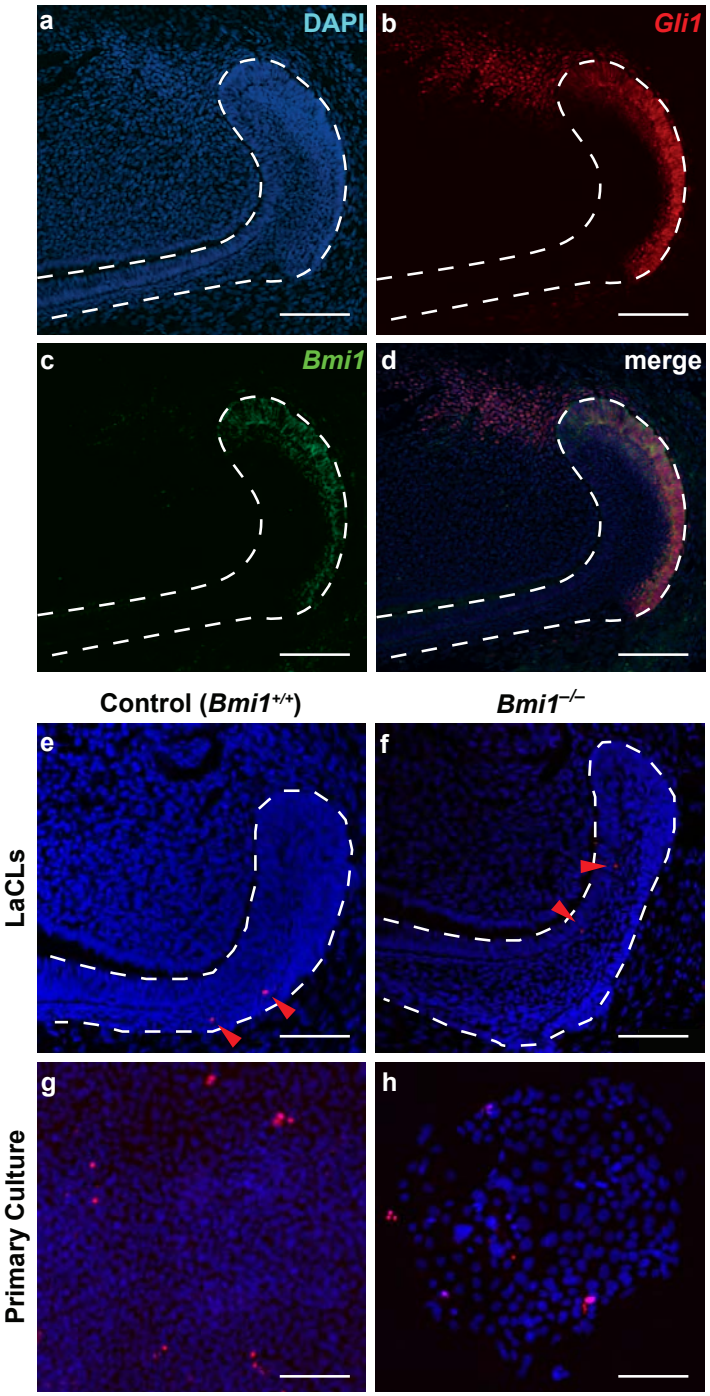

Figure S1 *Bmi1*^{GFP} **and** *Gli1*^{lacZ} expression overlap in the LaCL, and *Bmi1* is not required for cell survival. (**a**) DAPI, (**b**) *Gli1*^{lacZ}, and (**c**) *Bmi1*^{GFP} are merged in (**d**); *Bmi1*^{GFP} and *Gli1*^{lacZ} expression are coincident in the LaCL. (**e**,**f**) Removal of *Bmi1* does not result in increased apoptosis (red arrowheads), as detected by TUNEL staining. (**g**,**h**) No increased apoptosis is observed in *in vitro* cultured primary cells from control or *Bmi1*$^{-/-}$ LaCLs. Scale bar = 100 μm.

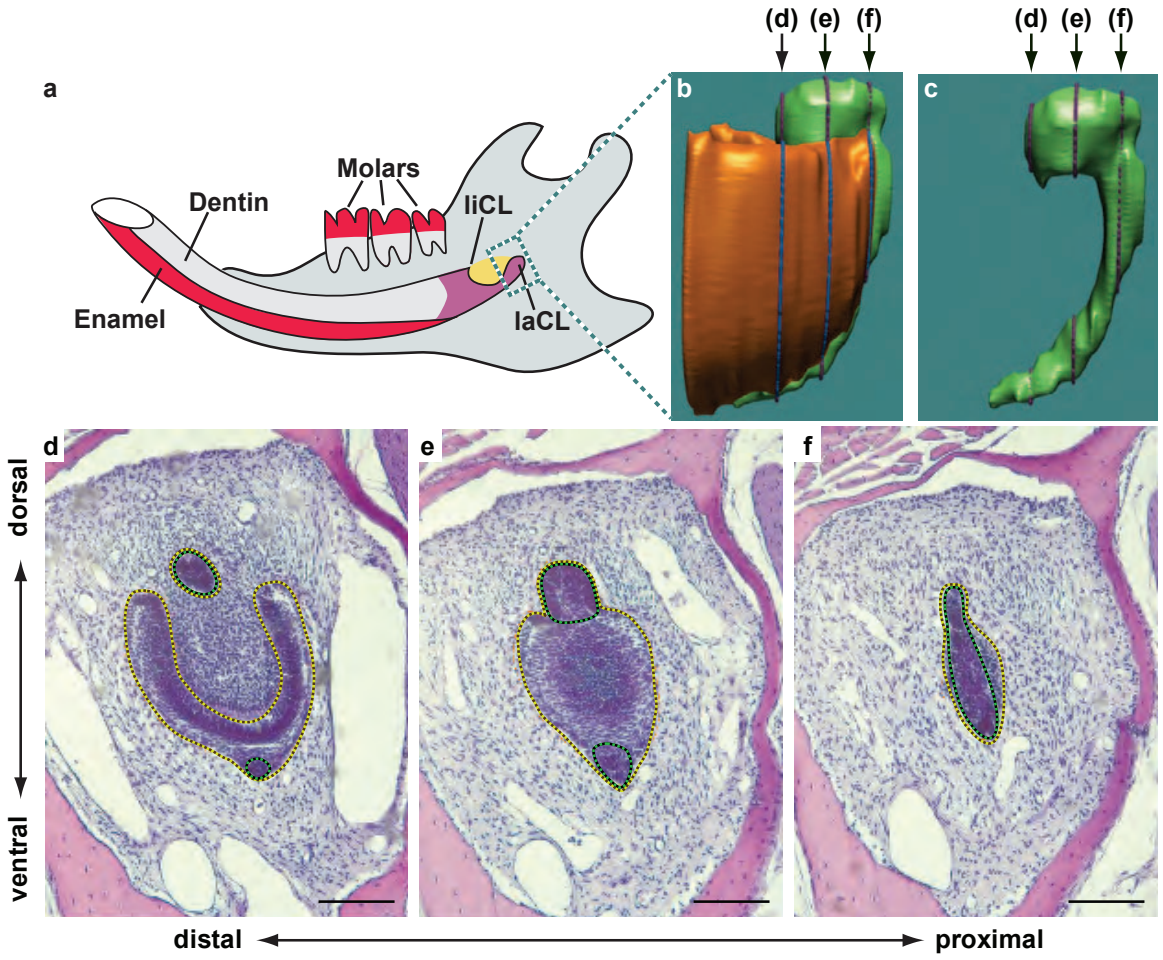

Figure S2 3-dimensional reconstruction of the LaCL. (**a**) Schematic diagram of an adult mandible. (**b**,**c**) The LaCL was reconstructed from serial sections of the proximal incisor. Examples are shown in (**d**,**e**,**f**). The bulbous region (green in **b**,**c**) of the LaCL can be distinguished from the rest of the epithelium (orange in **b**) based on cell morphology and density (green versus yellow dotted lines in **d**,**e**,**f**). Scale bar = 100 μm.

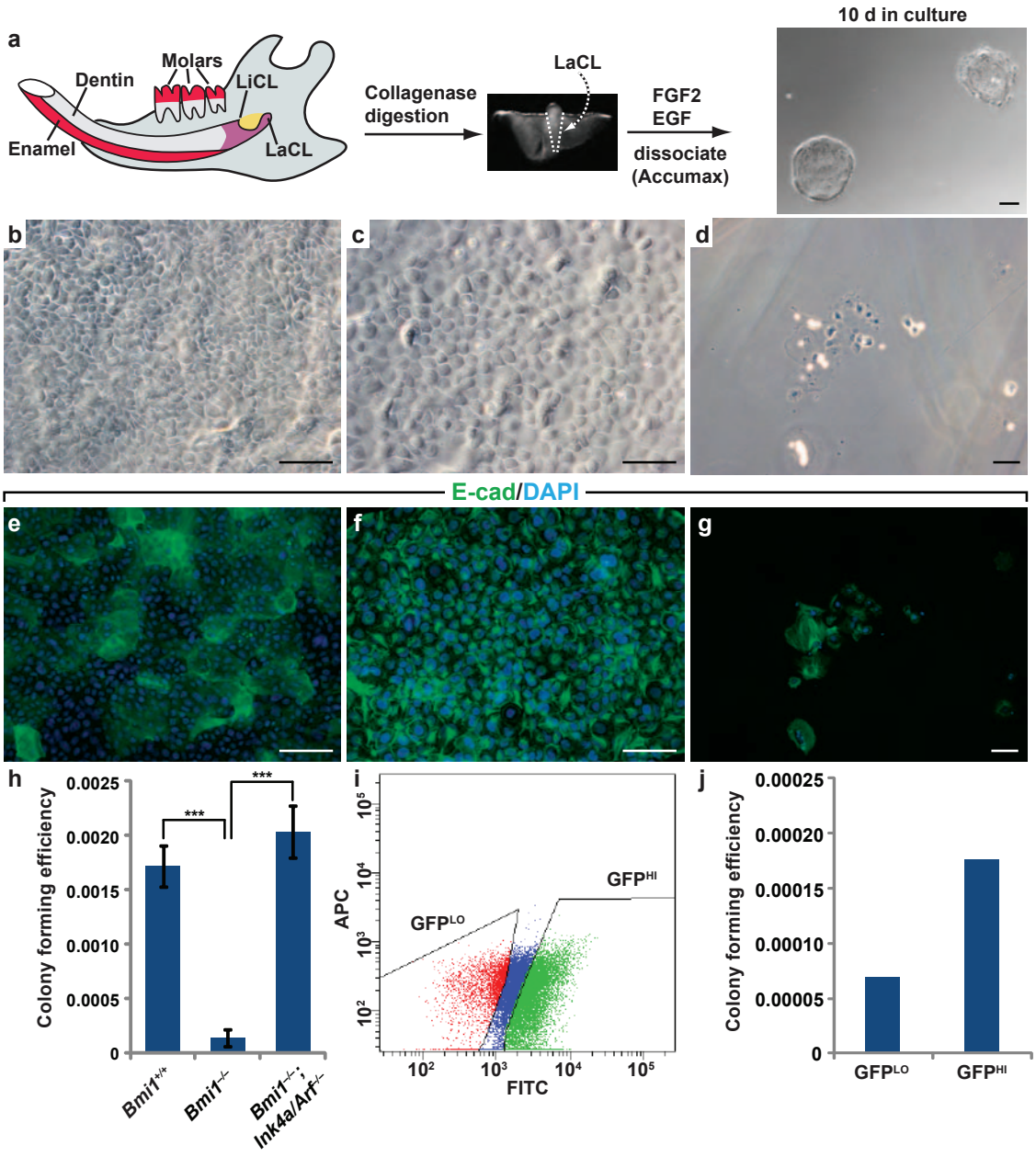

Figure S3 *Bmi1* is required for growth of primary LaCL cells *in vitro*. (**a**) Schematic depicting LaCL dissection, dissociation, and culture of LaCL cells. Ten days after plating, single stem cells proliferated to produce colonies. Different types of cultured LaCL cells can be identified based on cell morphology and growth rate (**b**-**d**) and expression of E-cadherin (**e**-**g**). (**h**) Stem cell colony formation by *Bmi1*$^{-/-}$ cells is impaired compared to WT cells but can be rescued by the removal of *Ink4a/Arf* (n = 4 control, 5 *Bmi1*$^{-/-}$, and 5 *Bmi1*$^{-/-}$;*Ink4a/Arf*$^{-/-}$ mice). (**i**,**j**) FACS sorted and plated cells from *Bmi1*^{GFP} LaCLs (GFP^{HI}) show an increase in colony forming efficiency compared to *Bmi1* negative cells that exhibit low GFP signal (GFP^{LO}) (n = 2 independent experiments). Error bars indicate means ± s.e.m. Source data of statistical analysis are shown in Supplementary Table S6 and S7. Scale bar = 100 μm.

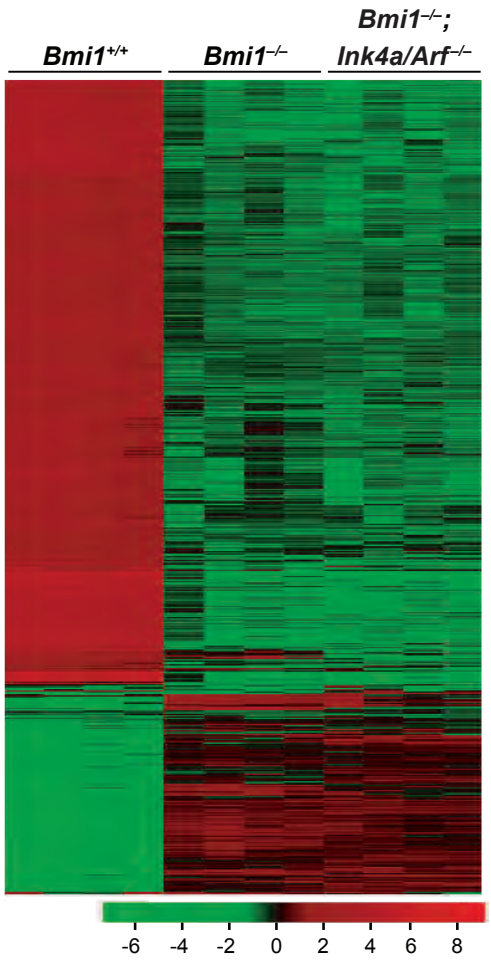

Figure S4 Microarray analysis showing gene expression in control (*Bmi1*$^{+/+}$), *Bmi1*$^{-/-}$, and *Bmi1*$^{-/-}$*;Ink4a/Arf*$^{-/-}$ colonies. The *Bmi1*$^{-/-}$*;Ink4a/Arf*$^{-/-}$ colonies exhibited an expression profile that was more similar to *Bmi1*$^{-/-}$ than control.

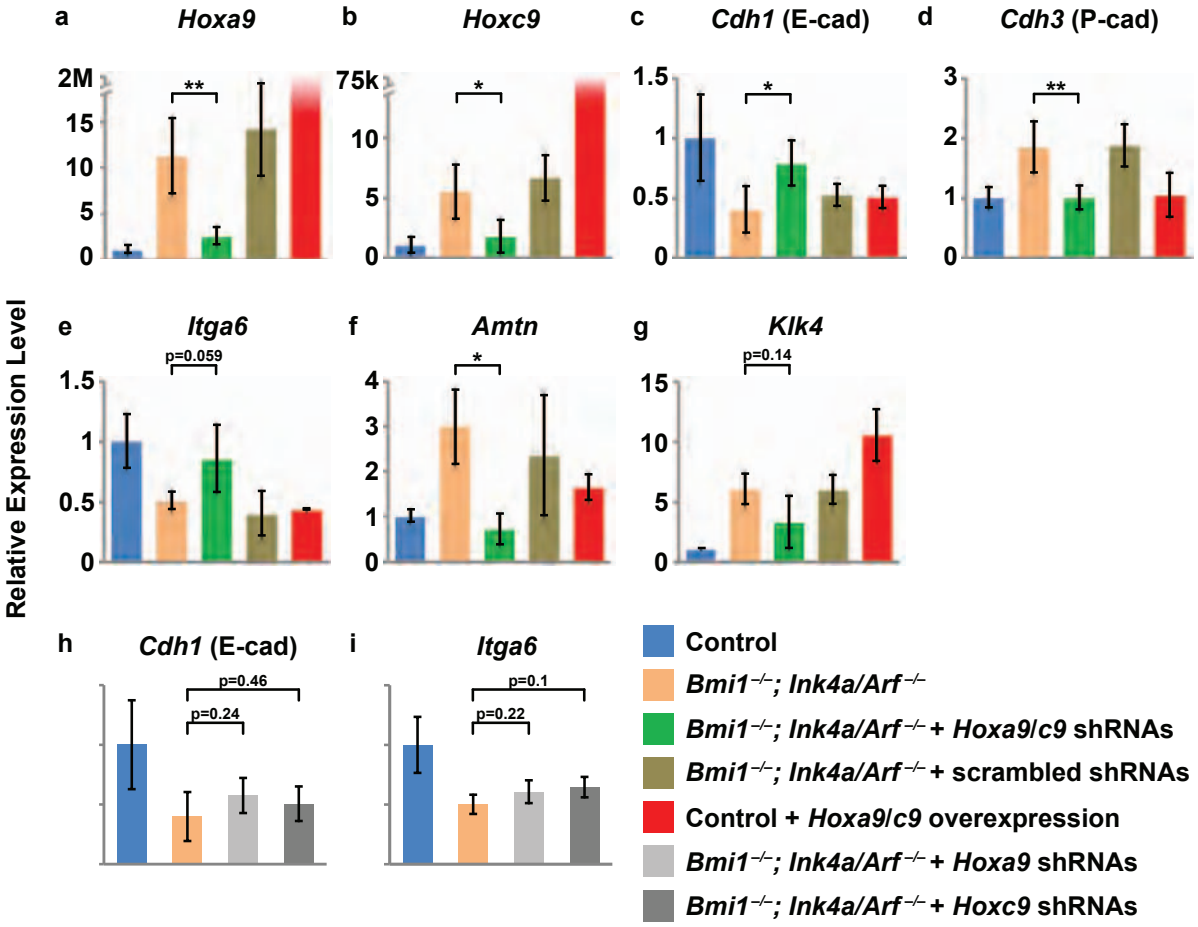

Figure S5 Relative expression level by qPCR of selected genes in cells cultured under different conditions. (**a**-**g**) *Hoxa9*, *Hoxc9*, *Cdh1*, *Cdh3*, *Itga6*, *Amtn*, and *Klk4* expression is restored to the control level by a second set of shRNAs against *Hoxa9* and *Hoxc9* but not by scrambled shRNAs. (**h**,**i**) However, single knockdown of *Hoxa9* or *Hoxc9* is insufficient to restore *Cdh1* and *Itga6* expression level (n = 3 independent experiments). Error bars indicate means ± s.d. * is $p < 0.05$, and ** is $p < 0.001$. Source data of statistical analyses are shown in Supplementary Table S5.

Supplementary Table Legends

Supplementary Table S1. Gene ontology. Gene ontology analysis reveals upregulation of genes normally involved in developmental processes and cell differentiation. Please also refer to Figure 3c.

Supplementary Table S2. Volumes of the LaCL stem cell compartments. 3D renderings from coronal sections enable reconstruction and measurement of the control, *Bmi1*$^{-/-}$, and *Bmi1*$^{-/-}$*;Ink4a/Arf*$^{-/-}$ LaCL volume. Please also refer to Figure 2v.

Supplementary Table S3. Numbers of BrdU label retaining cells in the LaCLs. BrdU positive cells are scored from sagittal sections through entire LaCLs from control, *Bmi1*$^{-/-}$, and *Bmi1*$^{-/-}$*;Ink4a/Arf*$^{-/-}$ animals. Please also refer to Figure 2w.

Supplementary Table S4. Cell sizes of cultured primary LaCL stem cells. LaCL stem cells from control or *Bmi1*$^{-/-}$*;Ink4a/Arf*$^{-/-}$ are cultured in the presence or absence of *Hoxa9*/*c9* RNAi or *Hoxa9*/*c9* cDNA. Cell sizes are measured using ImageJ. Please also refer to Figure 4f.

Supplementary Table S5. Relative expression level by qPCR of *Hoxa9*, *Hoxc9*, *Cdh1*, *Cdh3*, *Itga6*, *Amtn*, and *Klk4* in cells cultured under different conditions. LaCL stem cells from control or *Bmi1*$^{-/-}$*;Ink4a/Arf*$^{-/-}$ are cultured in the presence or absence of *Hoxa9*/*c9* RNAi or *Hoxa9*/*c9* cDNA. mRNA are collected for qPCR analysis. Please also refer to Figure 4g-m, and Supplementary Figure S5.

Supplementary Table S6. Colony forming efficiency. LaCL stem cells from control, *Bmi1*$^{-/-}$ and *Bmi1*$^{-/-}$*;Ink4a/Arf*$^{-/-}$ animals are cultured and colonies formed are counted. Please also refer to Supplementary Figure S3h.

Supplementary Table S7. Colony forming efficiency after FACS sorting. *Bmi1* positive and negative cells are FACS sorted, cultured, and formed colonies are counted. Please also refer to Supplementary Figure S3j.